Observation of nonlinear localized modes in an electrical lattice

P. Marquié,* J. M. Bilbault, and M. Remoissenet
Laboratoire de Physique de l'Université de Bourgogne, Phénomènes Non Linéaires, URA CNRS 1796, Faculté des Sciences, 6 Boulevard Gabriel, 21000 Dijon, France
(Received 21 February 1995)

We study a discrete electrical lattice where the dynamics of modulated waves can be modeled by a generalized discrete nonlinear Schrödinger equation that interpolates between the Ablowitz-Ladik and discrete-self-trapping equations. Regions of modulational instability (MI) are investigated and experimentally, we observe that MI can develop even for continuous waves with frequencies higher than the linear cutoff frequency of the lattice. These results are confirmed by the observation of "staggered" localized modes. Experimentally, it is finally shown that unlike envelope solitons, which can be observed close to the zero-dispersion point, the staggered modes experience strong lattice effects.

PACS number(s): 03.40.Kf, 84.40.Mk

I. INTRODUCTION

Ever since the discovery of solitons, there has been considerable interest in localized modes for spatially extended systems. In this context, intrinsic collapse to self-localized states [1–3] in nonlinear lattices is increasingly studied because of its wide significance in a great variety of physical systems. Contrary to the impurity-induced localized modes which can exist in linear lattices with impurities or disorder, these intrinsic localized modes can exist in nonlinear lattices without defects or disorder. The localized modes with frequencies above the band of the corresponding linearized systems and that have a staggered form, i.e, the neighboring sites oscillate out of phase, are particularly interesting. Remarkable properties of such modes have been discussed in a number of recent theoretical and numerical studies [3–7], but, to our knowledge, only one experimental investigation has been reported [8].

On another hand, discrete electrical transmission lines are very convenient tools to study the wave propagation in one-dimensional nonlinear dispersive media [9]. In particular, they provide a useful way to check how the nonlinear excitations behave inside the nonlinear medium and to model the exotic properties of new systems [10]. Moreover, nonlinear transmission lines (NLTLs) are potential candidates for a number of applications in the microwave range [11,12]. Like every nonlinear system, a NLTL can exhibit an instability that leads to a self-induced modulation of an input plane wave with the subsequent generation of localized pulses. This phenomenon is known as a Benjamin-Feir modulational instability (MI) and it is responsible of many physically interesting effects such as the formation of envelope solitons. In homogeneous nonlinear systems, MI may be considered as the leading mechanism for energy localization. In this context, we have shown recently [13,14] that envelope solitons can form related to the existence of MI in a NLTL. But, our theoretical analysis, based on the continuum limit approximation, e.g., described by a continuous nonlinear Schrödinger (NLS) equation, failed to describe the dynamics of the nonlinear waves in the regions of strong lattice effects, which may have a strong influence on MI conditions and the existence of localized modes.

It is the main purpose of the present paper to focus on the influence of discreteness in an experimental nonlinear transmission line. The paper is organized as follows. In Sec. II, we present a nonlinear electrical lattice where, to a first order approximation, the dynamics of modulated waves can be modeled by a generalized discrete nonlinear Schrödinger (DNLS) equation. This equation, which was introduced very recently by Kivshar *et al.* [6] and Cai *et al.* [7], interpolates between the integrable Ablowitz-Ladik [15] and discrete-self-trapping [16] models. We investigate the modulational instability as a function of the carrier wave frequency, in order to gain insight into the formation of localized states [17]. In Sec. III, we present the experimental results concerning the MI of a plane wave and discuss the validity of the theoretical model. Next, we study in detail the localized modes that have a "staggered" form. We compare their propagation properties to those of envelope solitons which can be observed for particular values of the carrier wave frequency. The effects of discreteness on the propagation of nonlinear wave packets are then presented. Finally, Sec. IV concludes the paper.

II. THEORY

We consider a lossless nonlinear electrical lattice made of N identical unit cells, as illustrated in Fig. 1. Each cell contains [13] a series linear inductance L_1 and a linear inductance L_2 in parallel with a nonlinear capacitor $C(V_n)$. Denoting by $Q_n(t)$ the nonlinear electrical charge of the nth cell and by $V_n(t)$ the corresponding voltage and using Krichhoff laws, we derive the system of nonlinear discrete equations

*Electronic address: marquie@satie.u-bourgogne.fr

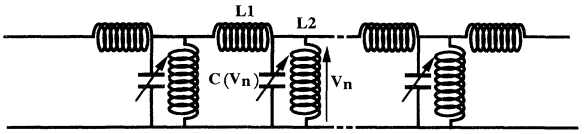

FIG. 1. Schematic representation of the experimental transmission line. The network is composed of $N=80$ identical cells, with two linear inductances L_1 and L_2. The nonlinear capacitance $C(V_n)$ consists of a varicap diode BB112 biased by a constant voltage (2 V) and connected in parallel with a linear capacitance $C_1=150$ pF.

$$\frac{d^2Q_n}{dt^2}=\frac{1}{L_1}(V_{n+1}+V_{n-1}-2V_n)-\frac{1}{L_2}V_n\ , \qquad n=1,2,\ldots,\ . \tag{2.1}$$

Furthermore, we assume (see experiments thereafter) that the charge has a voltage dependence similar to the one of an electrical Toda lattice [18,19]:

$$Q_n(t)=AC_0\ln\left[1+\frac{V_n}{A}\right]\ , \tag{2.2}$$

where A and C_0 are constants. This charge-voltage relation is verified if the inverse of the nonlinear capacitance obeys a linear relation [20]

$$\frac{1}{C(V_n)}=\frac{A+V_n}{AC_0}\ . \tag{2.3}$$

From (2.1), we easily get the linear dispersion relation of a typical bandpass filter

$$\omega^2=\omega_0^2+4u_0^2\sin^2\frac{k}{2}\ , \tag{2.4}$$

where $\omega_0^2=1/L_2C_0$ and $u_0^2=1/L_1C_0$. As displayed in Fig. 2, the corresponding linear spectrum has a gap $f_0=\omega_0/2\pi$ and it is limited by the cutoff frequency $f_{\max}=\omega_{\max}/2\pi=(\omega_0^2+4u_0^2)^{1/2}/2\pi$ due to lattice effects.

We focus now on the nonlinear behavior of the lattice. Replacing the expression for Q_n (2.2) in (2.1), we obtain

$$(A+V_n)\frac{d^2V_n}{dt^2}-\left[\frac{dV_n}{dt}\right]^2=\frac{u_0^2}{A}(A+V_n)^2\times\left[V_{n-1}+V_{n+1}-\left[2+\frac{\omega_0^2}{u_0^2}\right]V_n\right]\ . \tag{2.5}$$

In order to fully take into account the lattice discreteness, we assume that the gap angular frequency ω_0 is large with respect to the other frequencies of the system, i.e., $\omega_0^2\gg 4u_0^2$. This implies that, for a wave with any frequency f, all its harmonics lie above the cutoff frequency and, to a first approximation, can be neglected. Thus, restricting our study to slow temporal variations of the

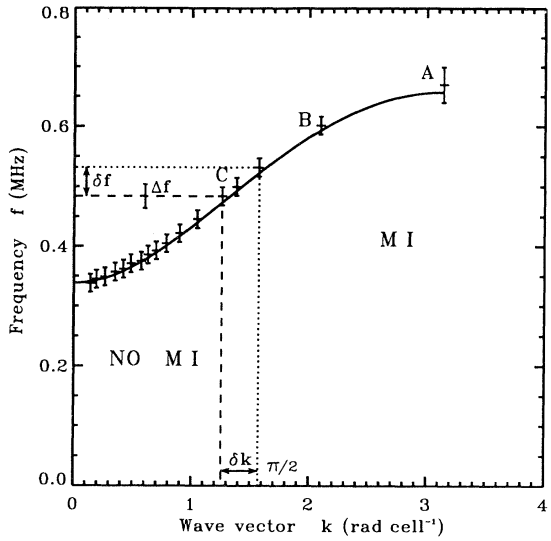

FIG. 2. Theoretical (continuous line) and experimental (crosses) linear dispersion curves. Modulational instability (MI) appears theoretically for $k>\pi/2$, that is, for $f>f_{\pi/2}=532$ kHz (dotted line), while experimentally (dashed line), a discrepancy of $\delta k=0.32$ rad cell^{-1} and $\delta f=(48\pm\Delta f)$ kHz ($\Delta f=20$ kHz) is observed.

wave envelope, we look for a solution of (2.5) in the form

$$V_n(t)=\varepsilon\Psi_n(T)e^{-i\omega t}+\varepsilon\Psi_n^*(T)e^{+i\omega t}\ , \tag{2.6}$$

where ε is a small parameter and $T=\varepsilon^2 t$. Inserting this expression in (2.5) and collecting dc terms of order ε^2, we obtain

$$\left[\Psi_{n+1}+\Psi_{n-1}-\left[2+\frac{\omega_0^2}{u_0^2}\right]\Psi_n\right]|\Psi_n|^2+\left[\Psi_{n+1}^*+\Psi_{n-1}^*-\left[2+\frac{\omega_0^2}{u_0^2}\right]\Psi_n^*\right]\Psi_n^2=-\frac{2\omega^2}{u_0^2}|\Psi_n|^2\Psi_n\ . \tag{2.7}$$

Next, collecting terms in $e^{-i\omega t}$, using (2.7), and setting $\tau=u_0^2T/2\omega$ and $\Psi_n=\Phi_n\exp[i\tau(\omega^2-\omega_0^2-2u_0^2)/u_0^2]$ yields

$$i\frac{d\Phi_n}{d\tau}+[\Phi_{n+1}+\Phi_{n-1}]+[\mu(\Phi_{n+1}+\Phi_{n-1})+2\nu\Phi_n]|\Phi_n|^2=0\ , \tag{2.8}$$

where the coefficients μ and ν are given by

$$\mu=\frac{1}{A^2}\ ,\qquad \nu=-\frac{2\omega^2+\omega_0^2+2u_0^2}{2u_0^2A^2}\ . \tag{2.9}$$

Equation (2.8), or the so-called IN-DNLS: integrable nonintegrable–discrete NLS equation, was recently stud-

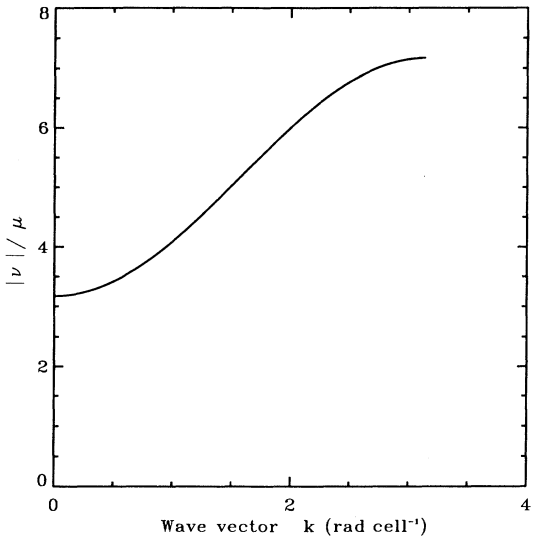

FIG. 3. Ratio $|\nu|/\mu$ vs wave number k.

ied by Kivshar *et al.* [6] and Cai *et al.* [7]. It reduces to the integrable Ablowitz-Ladik equation for $\nu=0$ and to the nonintegrable discrete NLS equation for $\mu=0$. Moreover, it was shown [7] that (2.8) can admit staggered localized modes solutions, i.e., localized modes with the neighboring sites oscillating out of phase. Note that for the real lattice we study, neither μ nor ν can be zero because their values are determined by those of the components. As can be seen in Fig. 3, the ratio $|\nu|/\mu$ versus the wave vector k varies from 3 to 7, so we are close neither to the Ablowitz-Ladik case nor to the discrete-self-trapping case.

Equation (2.8) has an exact continuous wave solution

$$\Phi_n(\tau)=\Phi_0 e^{-i(\omega\tau-kn)}, \tag{2.10}$$

where the angular frequency ω obeys the nonlinear dispersion relation

$$\omega=-2\cos k-2(\mu\cos k+\nu)\Phi_0^2 . \tag{2.11}$$

To analyze MI, which is responsible for energy localization, we seek a solution of (2.8) of the following form:

$$\Phi_n(\tau)=[\Phi_0+u_n(\tau)]e^{-i(\omega\tau-kn)}, \tag{2.12}$$

where $u_n(\tau)=a_n(\tau)+ib_n(\tau)$ is a small perturbation with angular frequency Ω and wave number K. Note that this perturbation acts simultaneously as amplitude modulation (a_n) and phase modulation (b_n). We then find that MI appears only if

$$\cos k\left[\Phi_0^2(\nu+\mu\cos k)-\sin^2\frac{K}{2}(1+\mu\Phi_0^2)\cos k\right]>0 . \tag{2.13}$$

Here, μ is always positive and ν is always negative. Consequently, from (2.13), we see that the continuous wave solution (2.10) will be unstable only in the region

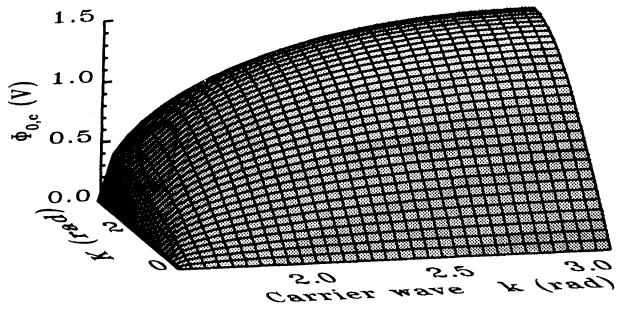

FIG. 4. Amplitude threshold $\Phi_{0,c}$ for modulational instability vs wave numbers k of the carrier wave and K of the perturbation.

$\pi/2<k<\pi$, provided that the amplitude Φ_0 exceeds the threshold $\Phi_{0,c}$ defined as follows:

$$\Phi_0^2>\Phi_{0,c}^2=\frac{|\cos k\sin^2(K/2)|}{|\nu+\mu\cos k\cos^2(K/2)|} . \tag{2.14}$$

Otherwise, that is, for $0<k<\pi/2$, the plane wave solution (2.10) remains stable. It is important to note that, contrary to what is found for the continuous NLS equation, the criterion (2.13) implies that the instability can occur for any value of the wave number K or corresponding frequency $F=\Omega/2\pi$ of the perturbation. The MI region is indicated in Fig. 2. The evolution of the threshold $\Phi_{0,c}$ versus the perturbation wave number K is presented in Fig. 4 for any value of the wave number k of the carrier wave ($\pi/2<k<\pi$). Here, we can notice that the more discreteness effects are important ($k\rightarrow k_{\max}=\pi$), the higher the necessary amplitude leading to MI.

III. EXPERIMENTAL RESULTS AND DISCUSSION

Our experiments are carried out on a nonlinear electrical lattice with $N=80$ cells. The linear inductances are $L_1=(680\pm14)$ μH and $L_2=(470\pm10)$ μH, whereas the Ohmic losses and inhomogeneities are small and can be ignored in a first approximation. The experimental arrangement is similar to the one described in Ref. [13], except for the nonlinear capacitance $C(V)$. Indeed, the inverse of the capacitance versus voltage has to fit the linear law (2.3) (see theory above). In practice, we have to connect a linear capacitance C_1 in parallel with the reverse-biased diode (BB112 Philips) previously used. The variations of $1/[C(V)+C_1]$ versus the voltage are well fitted by a straight line in the voltage range 0.5 to 4 V when 150 pF $\leq C_1 \leq$ 330 pF, and we have chosen $C_1=150$ pF. To sum up, the nonlinearity in the lattice is expressed by relation (2.2) with $A=3.9$ V and $C_0=(320+150)$ pF$=470$ pF.

The experimental linear dispersion curve shown in Fig. 2 agrees very well with the theoretical one, calculated with the above physical parameters. The experimental gap frequency f_0 and cutoff frequency $f_{\max}$ are, respectively, $f_0=340\pm15$ kHz and $f_{\max}=670\pm30$ kHz.

A. Modulational instability

Let us now check the theoretical predictions concerning the existence of MI in the system. Relation (2.13) predicts that MI can occur for $\pi/2 < k < \pi$, that is, for $f > f_{\pi/2} = 532$ kHz. When launching an initial plane wave whose frequency f is slightly modulated, we observe that if the amplitude is large enough, MI develops in the range 484 ± 20 kHz $\leq f \leq 700$ kHz, as recapitulated in Fig. 2. Now let us make the following remarks concerning these results. First, the external perturbation of the continuous wave, which becomes unstable if the MI conditions are verified, can be an amplitude modulation and/or a frequency modulation (see theory above). Here, we only consider frequency modulation, but amplitude modulation could be used (see [13]). Second, it has not been possible to determine experimentally the value of the amplitude threshold over which MI develops. At last, it is important to note that MI can develop in our system for frequencies $f < f_{\pi/2} = 532$ kHz contrary to the theoretical predictions. Then, the agreement between our model and our observations is not quite satisfactory. The reason for this discrepancy can be elucidated in the following way. Our theoretical analysis is based on the assumption that discreteness effects are strong, i.e., $\omega_0^2 \gg 4u_0^2$, or equivalently that $v_g \ll v_\varphi$ where $v_g = d\omega/dk$ and $v_\varphi = \omega/k$ are, respectively, the group velocity and the phase velocity in the system. As can be seen in Fig. 2, the gap ω_0 and allowed frequency bandwidths are in fact of the same order for our real network. Furthermore, by plotting the evolution of the ratio v_g/v_φ versus wave number k (see Fig. 5), we can verify that in the vicinity of $k = 1.25$ rad cell^{-1}, where v_g is maximum (zero-dispersion point), the condition $v_g \ll v_\varphi$ is no longer verified. This suggests that a semidiscrete approach is probably more appropriate to describe the dynamics of the wave envelope in the vicinity of the zero-dispersion point. In fact, by using such an approach, we can reduce (2.5) to the well known NLS equation

$$j\Phi_T + P\Phi_{XX} + Q|\Phi|^2\Phi = 0 , \tag{3.1}$$

with the coefficients $P = (u_0^2 \cos k - v_g^2)/2\omega$ and $Q = (u_0^2/\omega)(\nu + \mu \cos k)$. Then, the theoretical condition $PQ > 0$ for the existence of MI leads to $k > 1.25$ rad cell^{-1} that is $f > 478$ kHz. In the limit of our experimental precision, this value agrees very well with our measurements, since we have found that MI occurs for $f \geq 484 \pm 20$ kHz.

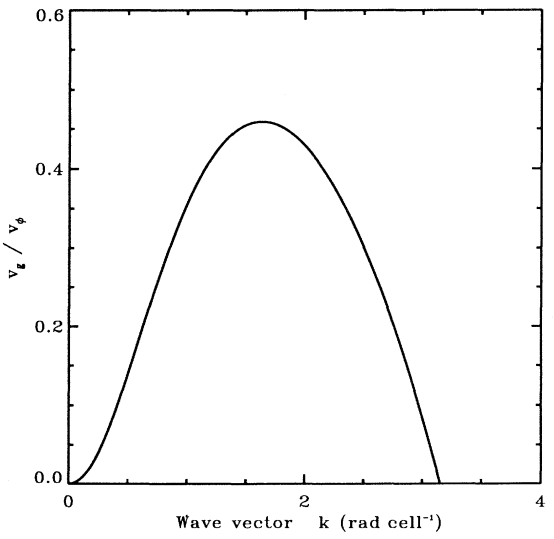

FIG. 5. Ratio v_g/v_φ vs wave vector k.

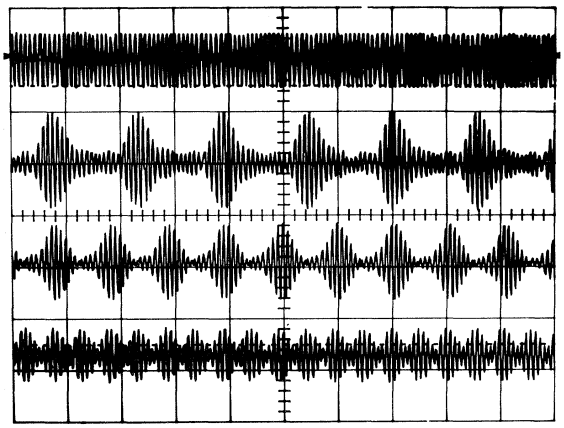

FIG. 6. Representation of the initial wave with constant amplitude and with $f = 600$ kHz (point B in Fig. 2), which is slightly frequency modulated (above, abscissa: 20 μs/division, ordinate: 2 V/division). The other oscillograms correspond to the observation at cell $n = 32$ of the self-modulated wave train for different modulation frequencies: $F = 32$, 48, and 96 kHz (abscissa: 20 μs/division, ordinate: 1 V/division).

To sum up, in the vicinity of the zero-dispersion point ($P \approx 0$), where v_g is maximum, the NLS equation (3.1) is more appropriate than the IN-DNLS equation (2.8) to describe the physics of the line. On the contrary, for strong lattice effects ($k \to \pi$), that is, when v_g becomes small, (2.8) is rather a good model.

Let us now examine MI for specific frequencies. For $f = 600$ kHz (point B in Fig. 2) MI, observed at cell $n = 32$, is represented in Fig. 6 for different values of the modulation frequency: $F = 32$, 48, and 96 kHz. This result is consistent with relation (2.13) which predicts that MI can develop in the same way for any value of the modulation frequency F. For $f = 700$ kHz (above point A in Fig. 2), MI at cell $n = 8$ is presented in Fig. 7 for $F = 900$ Hz; for the sake of clarity, only one period of the self-modulated wave train is displayed. In this case, MI occurs for a carrier wave with frequency $f > f_{\max}$ and the cells oscillate out of phase, as observed experimentally. It is important to note that the whole Fourier spectrum is concentrated above $f_{\max}$. This is, to our knowledge, the first observation of modulational instability outside the linear spectrum of a real system. Our main results concerning MI are also reported in Table I.

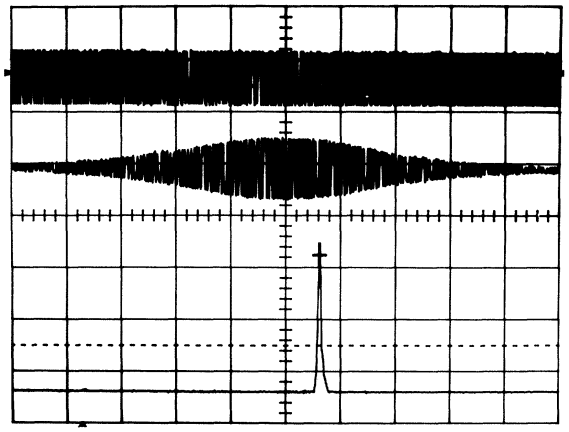

FIG. 7. Modulational instability for $f > f_{max}$ (above point A in Fig. 2). The initial wave with $f = 700$ kHz is slightly frequency modulated with $F = 900$ Hz (above, abscissa: 50 μs/division, ordinate: 2 V/division). One period of the corresponding wave at cell $n = 8$ is represented (abscissa: 50 μs/division, ordinate: 0.1 V/division) as is also its Fourier spectrum which presents a maximum at frequency 700 kHz (abscissa: 50 kHz/division, ordinate: 15 mV/division).

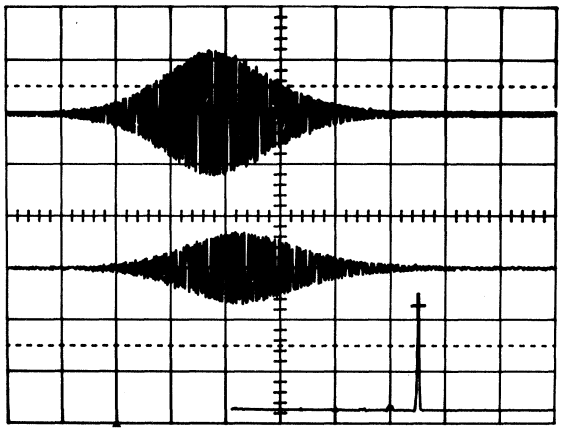

FIG. 8. Oscillograms of a staggered mode observed at cells $n = 3$ and $n = 8$ (downwards), with frequency $f = 680$ kHz (above option A in Fig. 2; abscissa: 50 μs/division, ordinate: 0.2 V/division). The corresponding Fourier spectrum (at cell $n = 8$), with width 20 kHz, is concentrated above f_{max} (abscissa: 100 kHz/division, ordinate: 15 mV/division).

B. Localized excitations and lattice effects

The above MI results suggest that localized wave packets with frequency f in the range 484 ± 20 kHz $\leq f \leq 700$ kHz probably exist. In the following, for convenience, we will use the terms "staggered mode" and "envelope soliton" for wave packets with wave number $k = \pi$ and $k \approx \pi/2$, respectively. Elsewhere, that is for $\pi/2 \leq k \leq \pi$, we will use the term "localized mode." From the above MI results, we expect staggered modes above the cutoff frequency, i.e., above point A in Fig. 2. Experimentally, these modes can be created by generating an initial wave packet of appropriate frequency at the input of the line. Figure 8 shows the oscillograms of a staggered mode ($k = \pi$) at cells $n = 3$ and 8. Its Fourier spectrum (at cell $n = 8$) is centered at frequency $f = 680$ kHz and has full width $\Delta f = 20$ kHz. As for MI, the whole spectrum is concentrated above the linear cutoff frequency $f_{max} = 670$ kHz. Such a mode moves very slowly, with average velocity $v_a \approx 0.14$ cell μs^{-1}. We have further observed that it gradually slows down and decays owing to strong lattice effects. The wave form recorded at cell $n = 8$ is well fitted by a sech function (not presented here). The temporal width measured at half height is $\Delta t \approx 110$ μs. The corresponding spatial width is $\Delta n = v_a \Delta t \approx 16$ cells. These results, which show for $k = \pi$ the existence of a sech-shaped localized mode with large width and small amplitude, agree with the behavior predicted by the approximate solutions [7] of Eq. (2.8).

We have tried to create a narrow staggered localized mode by launching a wave packet with initial frequency $f = 680$ kHz, wave number $k = \pi$, and width $\Delta t = 2$ μs. In this case, the initial wave packet evolves spontaneously into a wave packet with width $\Delta t = 5$ μs (at cell $n = 16$), which propagates at average velocity $v_a' \approx 1$ cell μs^{-1} and has a spatial width $\Delta_n' \approx 5$ cells. However, its spectrum with central frequency $f' = 510$ kHz (note that the initial one was $f = 680$ kHz) is now very large and spreads over the whole linear bandpass. Moreover, two neighboring cells oscillate now in quadrature, that is with wave number $k' = \pi/2$. Thus, we have not obtained a staggered mode but a wave packet whose formation mechanism has

TABLE I. Nonlinear behavior of the specific points A, B, and C (see Fig. 2) discussed in the text.

Specific points (see Fig. 2)	Point A $k = \pi$ rad s^{-1} $f = f_{max} = 670$ kHz	Point B $k = 2.1$ rad s^{-1} $f = 600$ kHz	Point C $k = 1.4$ rad s^{-1} $f = 500$ kHz
Theoretical model	IN-DNLS	IN-DNLS	continuous NLS
MI	yes and for $f \geq f_{max}$	yes	yes
Typical wave packet	staggered localized mode	localized mode	envelope soliton
Average velocity	0.14 cell μs^{-1}	0.7 cell μs^{-1}	1 cell μs^{-1}
Energy barrier (arb. units)	4	0.75	0

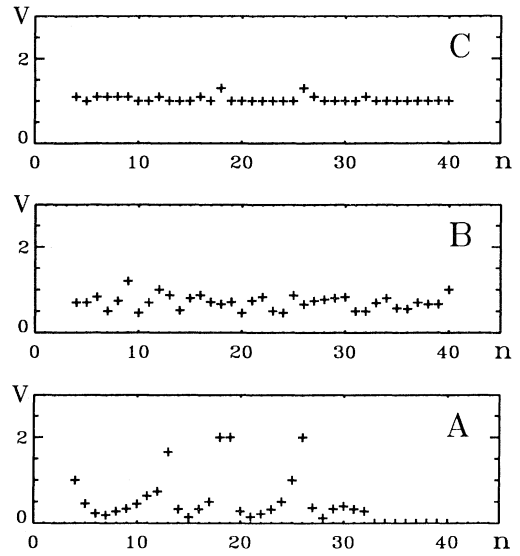

FIG. 9. Plot of the velocity of the "center of mass" (in cell μs^{-1}) vs the cell number n of an envelope soliton (point C in Fig. 2), a moving localized mode (point B), and a staggered mode (point A).

not been elucidated. It is then impossible to create narrow staggered localized modes which cover only a few sites, which at the same time have a Fourier spectrum concentrated above the cutoff frequency.

Next, for $f=600$ kHz (point B in Fig. 2), we have observed the translation of a localized mode, with average velocity $v_b \approx 0.7$ cell μs^{-1} (see velocity fluctuations hereafter), width $\Delta n \approx 11.2$ cells, and a sech-shaped wave form.

Otherwise, in the vicinity of the zero-dispersion point (point C in Fig. 2), the physics is described by the NLS equation (3.1) which admits envelope-soliton solutions. Indeed, for $f=500$ kHz, we have observed the free propagation of a sech-shaped envelope soliton with velocity $v_c=1$ cell μs^{-1} and width $\Delta n \approx 15.2$ cells.

In order to gain insight into the discreteness effects, which increase from point C to point A on the dispersion curve presented in Fig. 2, we have carefully measured the velocity v of the "center of mass" (which is approximately the velocity at maximum amplitude) of the moving modes corresponding to points C, B, and A. A plot of v as function of cell number n clearly shows that, unlike the envelope soliton [Fig. 9(c)] which propagates freely with constant velocity $v \approx v_g$, the velocity fluctuations increase with lattice dispersion as measured for the moving localized mode [Fig. 9(b)]. They are maximum for the staggered localized mode with $f=f_{\max}$ [Fig. 9(a)] where the neighboring cells oscillate out of phase, the maximum and minimum values of the velocity being, respectively, $v_{\max} \approx 2$ cell μs^{-1} and $v_{\min} \approx 0.15$ cell μs^{-1}. For the sake of clarity, these experimental results are also summarized in Table I.

Theoretically, it was known up to now that when a wave packet travels along a lattice, it experiences a periodic Peierls-Nabarro (PN) potential which becomes more and more pronounced with the increase of lattice effects. Here, we attribute the velocity fluctuations to the existence of a PN potential but, as can be seen from Figs. 9(b) and 9(a), in the limit of our experimental precision, it is not possible to detect any signature of the potential periodicity. This results agrees with a recent study in which Flach and Willis [21] have demonstrated that it was generally impossible to define a Peierls-Nabarro potential in order to describe the motion of a localized excitation through a lattice. Nevertheless, our results are indicative of an energy barrier E that we estimate to be $E \approx v_{\max}^2 - v_{\min}^2$ (kinetic energy difference). Thus, we have found $E \approx 4$ for the staggered mode, $E \approx 0.75$ for the moving localized mode, and $E \approx 0$ for the envelope soliton [on, respectively, Figs. 9(a), 9(b), and 9(c)]. These experimental results (see also Table I) clearly indicate that the energy barrier E increases with discreteness effects. In other terms, the wave packet loses gradually its soliton behavior in order to approach a localized mode behavior.

IV. CONCLUSION

In conclusion, we have studied the influence of discreteness in a real nonlinear electrical lattice. Theoretically, we have shown that the system of nonlinear equations governing the physics of the electrical network can be approximated by a generalized discrete nonlinear Schrödinger equation which interpolates between the Ablowitz-Ladik and discrete-self-trapping equations. From this analysis, the possibilities for the system to present modulational instability have been investigated.

Experimentally, we have observed that MI can occur in a larger region than the predicted one. The discrepancy between the theoretical and experimental limits for MI has been elucidated by using a semidiscrete approach leading to a continuous NLS model, which is more appropriate for our real network in the vicinity of the zero-dispersion point. More importantly, we have the following:

(i) We have observed MI for frequencies above the linear cutoff frequency $f_{\max}$ of the system.

(ii) These results have been confirmed by the observation of staggered localized modes ($k=\pi$) for which the whole frequency spectrum is concentrated above $f_{\max}$.

(iii) Concerning the propagation of nonlinear wave packets, we have shown that unlike the envelope soliton which can propagate with constant velocity, the localized modes undergo velocity fluctuations due to lattice dispersion when they propagate. These effects become maximum for the staggered localized modes which can propagate only along a few cells.

Finally, our electrical network is very convenient to study the nonlinear dynamics of nonlinear lattices. Indeed, by an appropriate choice of the frequency, we can shift progressively from the continuous NLS behavior to the discrete IN-DNLS behavior. Furthermore, our results also suggest that localized wave packets should be investigated in other systems such as atomic or molecular lattices.

ACKNOWLEDGMENT

The authors are grateful to B. Michaux for his invaluable technical assistance.

[1] A. J. Sievers and S. Takeno, Phys. Rev. Lett. **61**, 970 (1988).
[2] J. B. Page, Phys. Rev. B **41**, 7835 (1990).
[3] S. Takeno, J. Phys. Soc. Jpn. **61**, 2821 (1992).
[4] K. W. Sandusky, J. B. Page, and K. E. Schmidt, Phys. Rev. B **46**, 6161 (1992).
[5] S. R. Bickman, S. A. Kisilev, and A. J. Sievers, Phys. Rev. B **47**, 14 206 (1993).
[6] Y. S. Kivshar and M. Salerno, Phys. Rev. E **49**, 3543 (1994).
[7] D. Cai, A. R. Bishop, and N. Grønbech-Jensen, Phys. Rev. Lett. **72**, 591 (1994).
[8] B. Denardo, B. Galvin, A. Greenfield, A. Larraza, S. Putterman, and W. Wright, Phys. Rev. Lett. **68**, 1730 (1992).
[9] A. C. Scott, *Active and Nonlinear Wave Propagation in Electronics* (Wiley-Interscience, New York, 1970).
[10] K. E. Lonngren, in *Solitons in Action,* edited by K. E. Lonngren and A. C. Scott (Academic, New York, 1978).
[11] D. Jäger, Int. J. Electron. **58**, 649 (1985).
[12] M. J. W. Rodwell, S. T. Allen, R. Y. Yu, M. G. Case, U. Bhattacharya, M. Reddy, E. Carman, M. Kamegawa, Y. Konishi, J. Pusl, and R. Pullela, Proc. IEEE **82**, 1037 (1994).
[13] P. Marquié, J. M. Bilbault, and M. Remoissenet, Phys. Rev. E **49**, 828 (1994).
[14] J. M. Bilbault, P. Marquié, and B. Michaux, Phys. Rev. E **51**, 817 (1995).
[15] M. J. Ablowitz and J. M. Ladik, J. Math. Phys. **17**, 1011 (1976).
[16] J. C. Eilbeck, P. S. Lomdahl, and A. C. Scott, Physica D **16**, 318 (1985).
[17] Y. S. Kivshar and M. Peyrard, Phys. Rev. A **46**, 3198 (1992).
[18] R. Hirota and K. Suzuki, Proc. IEEE **61**, 1483 (1973).
[19] M. Toda, *Theory of Nonlinear Lattices* (Springer-Verlag, Berlin, 1978).
[20] M. Remoissenet, *Waves Called Solitons* (Springer-Verlag, Berlin, 1994).
[21] S. Flach and C. R. Willis, Phys. Rev. Lett. **72**, 1777 (1994).